JOURNAL OF GEOPHYSICAL RESEARCH, VOL. 115, A05209, doi:10.1029/2008JA013948, 2010

Penetration of the convection and overshielding electric fields to the equatorial ionosphere during a quasiperiodic *DP* 2 geomagnetic fluctuation event

T. Kikuchi,[1,5] Y. Ebihara,[2] K. K. Hashimoto,[3] R. Kataoka,[4] T. Hori,[1] S. Watari,[5] and N. Nishitani[1]

Received 26 November 2008; revised 17 October 2009; accepted 17 November 2009; published 15 May 2010.

[1] The convection electric field penetrates to the equatorial ionosphere with no significant shielding during *DP* 2 fluctuation events with periods of 30–60 min (Nishida, 1968) and even during the main phase of a storm that continues over several hours (Huang et al., 2007). On the other hand, shielding becomes effective in 20 min during the substorm growth phase (Somayajulu et al., 1987), and in 1 h during the main phase of a storm (Kikuchi et al., 2008a). To clarify the relative contributions of the convection and shielding electric fields at middle to equatorial latitudes, we analyzed an equatorial *DP* 2 fluctuation event of 30 min duration, using magnetometer data, Super Dual Auroral Radar Network (SuperDARN) convection maps, and electric potentials calculated with the comprehensive ring current model (CRCM). The equatorial *DP* 2 fluctuations were found to be caused by alternating eastward electrojets (e-EJ) and westward electrojets (w-EJ) in the equatorial ionosphere, which were caused by the southward and northward interplanetary magnetic field, respectively. Using the SuperDARN convection map, we further show that the e-EJ is associated with large-scale two-cell convection vortices, while the w-EJ accompanies reverse flow vortices equatorward of the two-cell vortices. With the aid of the CRCM, we suggest that the reverse flow vortices were associated with the region 2 field-aligned currents (R2 FACs) that caused overshielding at the equator. We think it reasonable that the overshielding electric field could appear at middle to equatorial latitudes irrespective of the period of fluctuations as the region 1 FACs decrease their intensity. This scenario well explains both *DP* 2 fluctuations with periods of 30–60 min and continuous penetration for several hours during the main phase of storms.

Citation: Kikuchi, T., Y. Ebihara, K. K. Hashimoto, R. Kataoka, T. Hori, S. Watari, and N. Nishitani (2010), Penetration of the convection and overshielding electric fields to the equatorial ionosphere during a quasiperiodic *DP* 2 geomagnetic fluctuation event, *J. Geophys. Res.*, *115*, A05209, doi:10.1029/2008JA013948.

1. Introduction

[2] Quasiperiodic *DP* 2 magnetic fluctuations with periods of 30–60 min appear coherently at high latitude and the dayside geomagnetic equator; they are characterized by twin current vortices at high latitude and zonal current at the equator [*Nishida et al.*, 1966]. *Nishida* [1968] found that the *DP* 2 fluctuations were coherent with those in the southward interplanetary magnetic field (IMF) in such a manner that the ground magnetic H component increased as the IMF turned southward and decreased as it turned northward. *Nishida* [1968] pointed out that this coherency was observed even when the IMF B_z was mostly positive. However, because of large variability of the diurnal magnetic field variation on disturbed days, it was not determined whether the decreasing part of the equatorial *DP* 2 fluctuations was caused by a westward electrojet (w-EJ). In fact, the daytime geomagnetic field was often much lower than the quiet-time level [*Matsushita and Balsley*, 1972; *Onwumechilli et al.*, 1973; *Kikuchi et al.*, 1996]. *Matsushita and Balsley* [1972] suggested that *DP* 2 fluctuations should be measured as negative from the quiet-time level. *Kikuchi et al.* [1996], on basis of the high correlation coefficient (0.9) between high-latitude and equatorial *DP* 2 fluctuations, confirmed Nishida's scenario that the *DP* 2 fluctuations should be measured as positive from the smoothed diurnal variation, which was

[1]Solar-Terrestrial Environment Laboratory, Nagoya University, Nagoya, Japan.
[2]Advanced Research Institute, Nagoya University, Nagoya, Japan.
[3]Kyushu University of Health and Welfare, Nobeoka, Japan.
[4]Computational Astrophysics Laboratory, Institute of Physics and Chemical Research (RIKEN), Wako, Japan.
[5]National Institute of Information and Communications Technology, Tokyo, Japan.

0148-0227/10/2008JA013948

superposed by a negative magnetic deflection, probably due to the disturbance dynamo [*Blanc and Richmond*, 1980].

[3] Nishida's results and subsequent analyses based on high time-resolution magnetometer data [*Kikuchi et al.*, 1996; *Kobea et al.*, 1998] showed no significant shielding effects during *DP* 2 fluctuations. Moreover, *Huang et al.* [2005], demonstrating that the convection electric field was observed at the dayside equator during the entire period of the main phase of a storm, concluded that the shielding did not work for several hours during the storm main phase.

[4] Although it seems reasonable that the convection electric field penetrates to the equator for several hours [*Huang et al.*, 2005], there has been much evidence and theoretical explanation for the shielding/overshielding electric field at the equator [*Kelley et al.*, 1979; *Gonzales et al.*, 1979; *Fejer et al.*, 1979; *Kobea et al.*, 2000; *Kikuchi et al.*, 2000, 2003; *Vasyliunas*, 1972; *Jaggi and Wolf*, 1973; *Southwood*, 1977; *Senior and Blanc*, 1984; *Peymirat et al.*, 2000]. The shielding electric field is produced by completion of a current circuit between the ionosphere and the asymmetric ring current via the region 2 field-aligned current (R2 FAC) [*Vasyliunas*, 1972]. The shielding time constant deduced from magnetometer observations was 17–20 min [*Somayajulu et al.*, 1987; *Kikuchi et al.*, 2000] and that deduced from model calculations was 20–30 min for typical ionospheric and magnetospheric parameters [*Senior and Blanc*, 1984]. Therefore, the shielding electric field must have contributed to some extent to the *DP* 2 fluctuations, the period of which lies in the range of the shielding time constant.

[5] The puzzling issue mentioned above should be clarified for better understanding of the penetration of the convection electric field, which plays a crucial role in the electrodynamics of the low-latitude ionosphere and ring current development in the inner magnetosphere. In particular, we need to clarify the role of the shielding/overshielding electric field in short-period geomagnetic perturbations. To address this issue, we selected a *DP* 2 fluctuation event with a period of 30 min, which was amplified at the dayside geomagnetic equator. We used magnetometer data at middle-latitude and low-latitude stations to obtain magnetic signatures attributable to the *DP* 2 ionospheric currents extending from high latitude to the equator. The low-latitude station provides data about magnetic perturbations caused by magnetospheric currents such as the magnetopause, tail, and field-aligned currents and the ring current. *DP* 2 fluctuations at the equator were attributed to alternating eastward electrojets (e-EJ) and w-EJ, caused by the southward and northward IMF, respectively. The e-EJ is thought to be driven by the dawn-to-dusk convection electric field associated with the region 1 field-aligned currents (R1 FACs), while the w-EJ should be caused by the overshielding electric field associated with the R2 FACs. To evaluate this hypothesis, we examined the Super Dual Auroral Radar Network (SuperDARN) convection map in the polar ionosphere for the period of the *DP* 2 fluctuation event. Moreover, we ran the comprehensive ring current model (CRCM) [*Fok et al.*, 2001], using the solar wind data as an input to examine relative contributions of the R1 and R2 FACs in the convection map. From the observational and simulation results, we conclude that the e-EJ and w-EJ responsible for the *DP* 2 fluctuations were caused by the R1 and R2 FACs, respectively. Furthermore, we show *DP* 2 fluctuation events with different properties to reinforce our conclusion and discuss the continuous penetration of the convection electric field for several hours during the main phase of a storm [*Huang et al.*, 2005, 2007] and overshielding during the storm recovery phase [*Kikuchi et al.*, 2008a, 2008b].

2. *DP* 2 Fluctuation Event on 14 December 2006

2.1. Interplanetary Magnetic Field and Geomagnetic Indices

[6] Figure 1 shows the interplanetary magnetic field components (B_x, B_y, and B_z) and solar wind velocity and density observed by Advanced Composition Explorer (ACE) satellite at $x = 1.452 \times 10^6$ km. The IMF B_z oscillated in the ULF range with large amplitude after the arrival of the shock at 1352 UT and then remained positive for 4 h. These IMF variations caused substorm activities over 4 h with $AL \leq -1500$ nT, as shown in Figure 2. The IMF B_z then fluctuated with a period of 30 min and ranging in magnitude from −12 to +15 nT for the period 2100–2300 UT, as indicated by the double-headed arrow in Figure 1. The oscillation in the IMF B_z caused the *AL* to oscillate quasiperiodically with a magnitude of 500 nT for the period of 2130–2330 UT, as indicated by the double-headed arrow in Figure 2. The IMF remained southward from 2230 UT with a magnitude of 15 nT, causing the *AL* to drop below −1000 nT; this caused the main phase of the geomagnetic storm on 14–15 December, as shown by the ring current index, SYM-H, in Figure 2.

2.2. Equatorial Electrojet

[7] Figure 3 shows *H* component magnetic fields at Paratunka, Russia (PTK, 45.58°N geomagnetic latitude (GML), Table 1), Okinawa, Japan (OKI, 16.87°N GML), and Yap, Micronesia (YAP, 0.38°S GML). The *H* component increased suddenly at 1414 UT, owing to increases in the solar wind density and velocity at 1352 UT and remained high for 1.5 h. The large amplitude of the *H* component at PTK peaking at 1500 UT must have been caused by a substorm wedge current, which closes with the westward auroral electrojet, represented by the decrease in *AL* (see Figure 2). The *H* component at OKI started to decrease at 2300 UT, indicating development of a storm ring current. Quasiperiodic fluctuations occurred at YAP during the period of 2130–2330 UT, as indicated by the double-headed arrow in Figure 3, before the ring current developed. These fluctuations correspond to those in *AL* (Figure 2) and in the IMF B_z (Figure 1). Similar fluctuations were observed at YAP in another time interval (0000–0300 UT), corresponding to those in *AL* during the main phase of the storm (Figure 2). These fluctuations were recorded at PTK and OKI with amplitudes smaller than those at YAP. The equatorial enhancement of the amplitude fluctuations verifies that the equatorial magnetic fluctuations were mainly caused by ionospheric currents amplified by the Cowling effect [e.g., *Kikuchi et al.*, 1996].

[8] Our primary purpose in using magnetometer data was to monitor the ionospheric currents and thereby deduce information about electric fields originating in the magnetosphere. The magnetic perturbations shown in Figure 3 contain several components, such as quiet-time diurnal

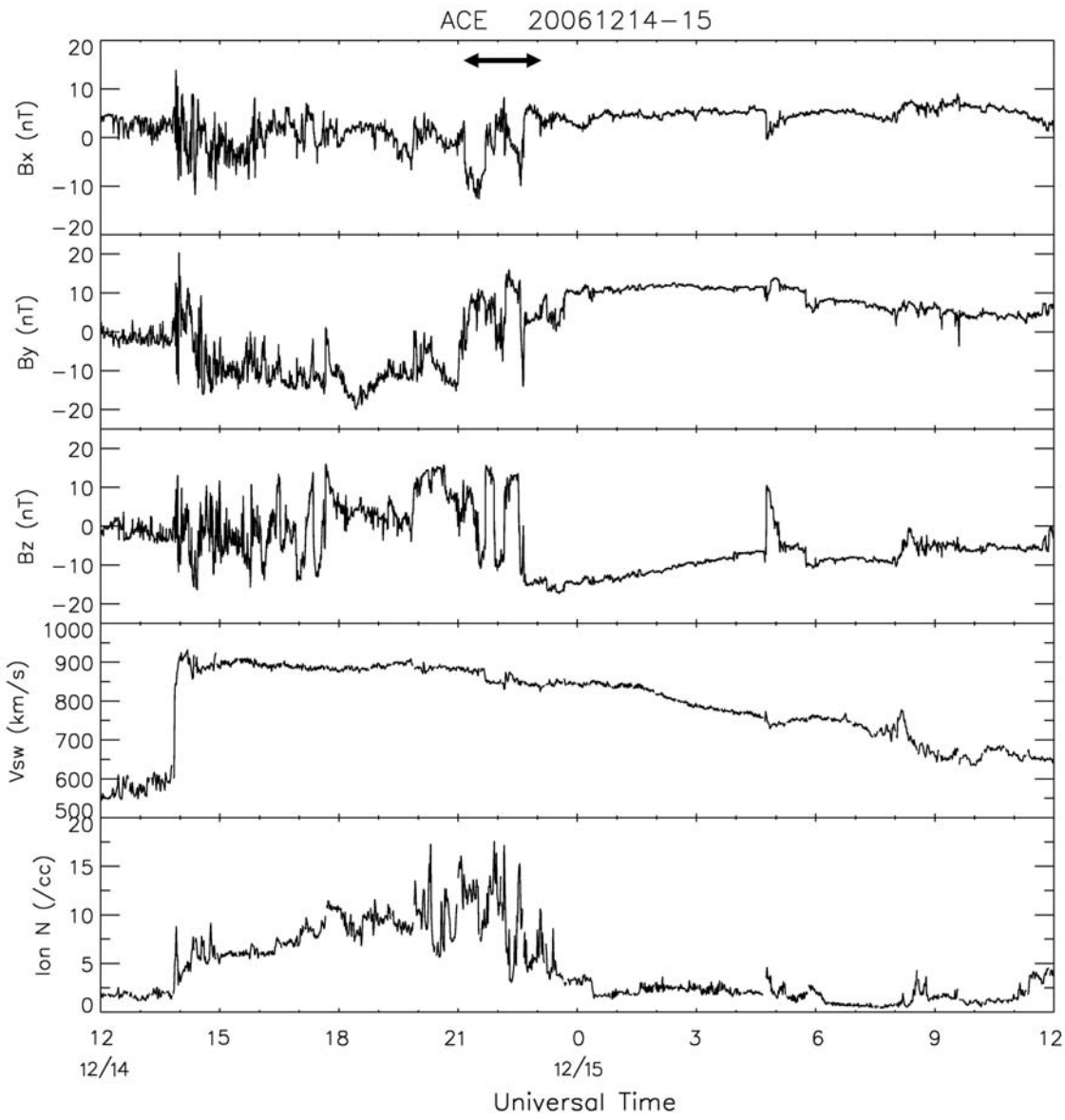

Figure 1. (top to bottom) Interplanetary magnetic field B_x, B_y, and B_z and solar wind velocity and density observed by ACE at 1.452×10^6 km s^{-1} for the period from 12 UT, 14 December 2006, to 12 UT, 15 December 2006. The IMF B_z fluctuated with a period of 30 min in a time interval of 21 to 23 UT, as indicated by the double-headed arrow.

variations and magnetic perturbations attributable to the magnetopause, tail, field-aligned, and ring currents. To determine the quiet-time diurnal variation, we plotted *H*, *D*, and *Z* components at YAP over the period 10–15 December 2006 in Figure 4. The diurnal curve in the *H* component is smooth on 10 December, at which time the SYM-H is greater than −20 nT. If we define this curve as a quiet-day curve, daytime levels around noon (0300 UT) are below the quiet-time curve (Figure 4, thin line) on disturbed days (Figure 4, thick line): 12–14 December. The depression of the daytime level raised the question of whether the *DP* 2 fluctuations were positive [*Nishida et al.*, 1966; *Nishida*, 1968, 1973] or negative [*Matsushita and Balsley*, 1972] with respect to the quiet-time curve. Depression of the daytime level is commonly observed on disturbed days, probably because of the disturbance dynamo electric field [e.g., *Fejer and Scherliess*, 1997]. Thus, we selected 10 December as a quiet day in the following analyses.

[9] As Figure 4 shows, the deflection from the quiet-time level is small in the time interval of 2100–2400 UT (0600–0900 magnetic local time (MLT)) on disturbed days, 12 and 13 December, because of small ionospheric conductivity under a large solar zenith angle. Note that no deflections are recognized around the beginning of the *DP* 2 fluctuation event (2200 UT on 14 December). We next assume that perturbations recorded at OKI were least influenced by ionospheric currents, since OKI was far from the auroral electrojets and outside of the equatorial electrojet. Assuming that YAP and OKI were similarly affected by magnetospheric currents, we subtract the perturbations at OKI from those at YAP after

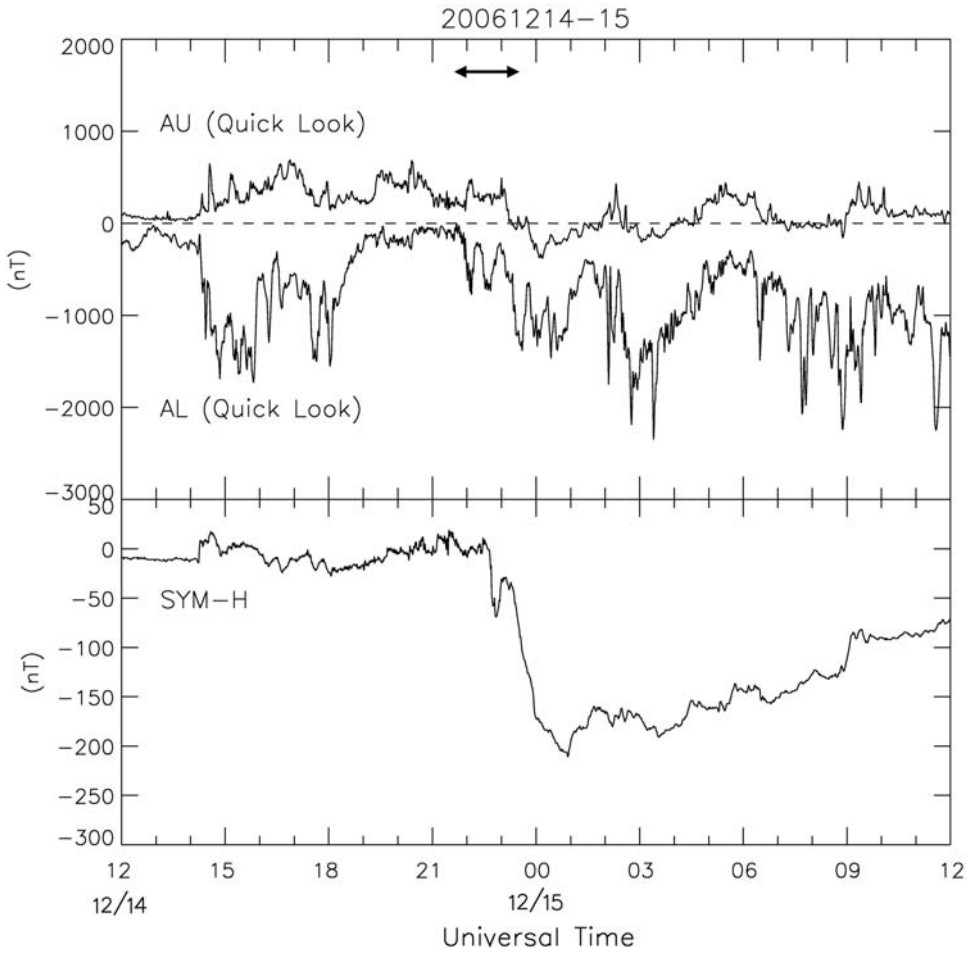

Figure 2. Auroral electrojet indices *AU* and *AL* and the ring current index SYM-H for the period from 12 UT, 14 December, to 12 UT, 15 December 2006. The geomagnetic sudden commencement started at 1414 UT, and the main phase started at around 23 UT on 14 December. The quasiperiodic fluctuations occurred during the period of 2130–2330 UT, as indicated by the double-headed arrow in the upper panel.

eliminating quiet-time diurnal variations at each station. This then yields the *DP* 2 fluctuations caused by ionospheric currents driven by the convection/overshielding electric fields.

[10] Figure 5 shows *DP* 2 fluctuations in a time frame from 1800 UT, 14 December, to 1200 UT, 15 December (Figure 5, bottom), together with the SYM-H (Figure 5, top). Note that the *DP* 2 fluctuations over the period 2130–2330 UT (double-headed arrow) are composed of alternating positive and negative magnetic deflections caused by e-EJ and w-EJ, respectively. An outstanding property of the *DP* 2 fluctuations is that the amplitude (>100 nT from peak to peak) is larger than the quiet-time diurnal variation (Figure 4). The large amplitude helps us to find that the *DP* 2 fluctuations are composed of alternating e-EJ and w-EJ. We also have fluctuations in a time interval of 0000–0300 UT, 15 December, superposed by a long-lasting negative deflection. These fluctuations might be related to inner magnetosphere disturbances, while the long-lasting negative deflection might be caused by the disturbance dynamo electric field which develops several hours after the onset of the storm [*Fejer and Scherliess*, 1997].

[11] Figure 6 shows *H*, *D*, and *Z* component magnetic fields at the midlatitude station, PTK, along with those at YAP in the time interval of 2100–2400 UT. Figure 6 (dotted lines) also plots quiet-time diurnal variations on 10 December 2006. We observe that the *H* component fluctuations at PTK are poorly correlated with those at YAP, but the *D* component fluctuations with positive peaks at 2210, 2235, and 2310 UT are well correlated with the *DP* 2. If we assume that the *D* component fluctuations at PTK are caused by ionospheric currents, the ionospheric currents should be a southward (northward) current in the morningside midlatitude ionosphere, which connects the equatorial e-EJ (w-EJ) with the field-aligned currents. The poor correlation of the *H* component at PTK may indicate that PTK was dominantly under the influence of the magnetospheric currents.

[12] We now compare the *DP* 2 fluctuations with solar wind parameters to clarify causes of the alternating e-EJ and w-EJ. *Nishida* [1968] attributed the *DP* 2 fluctuations to fluctuations in the southward IMF. However, we do not adopt this hypothesis a priori but attempt to find signatures indicating a cause-and-effect relationship between the solar wind parameters and the *DP* 2 fluctuations. We used high-

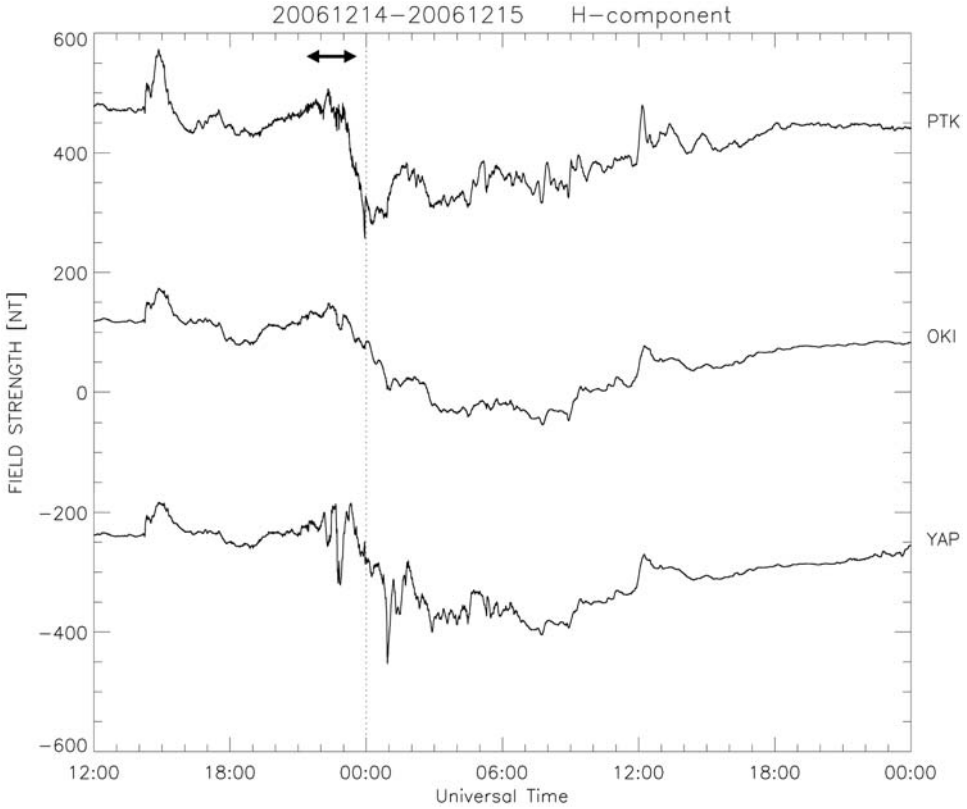

Figure 3. *H* component magnetic fields recorded at geomagnetic midlatitude, Paratunka, Russia (PTK, 45.58°N GML); geomagnetic low latitude, Okinawa, Japan (OKI, 16.87°N GML); and geomagnetic equator, Yap, Micronesia (YAP, 0.38°S GML), during the geomagnetic storm on 14–15 December 2006. Quasiperiodic *DP* 2 fluctuations are amplified at YAP during the period of 2130–2330 UT, as indicated by the double-headed arrow.

time-resolution (16 s) solar wind data and compared detailed structures with the equatorial *DP* 2 variations. Figure 7 shows the solar wind dynamic pressure (top), IMF B_z (middle), and the *DP* 2 fluctuations (bottom). As a result of careful comparisons, we shifted the time of the solar wind data by 32 min behind. From the solar wind velocity, 850 km s^{-1}, and the distance between the spacecraft and the magnetopause assumed at 10 R_E, we have 27.2 min for the propagation time of the solar wind. As a first step, we shifted the time in the solar wind data by 27.2 min and then attempted to find signatures in a cause-and-effect relationship. In carrying out these analyses, we focused our attention not only on IMF effects, but also to solar wind dynamic pressure effects. As is widely known, a solar wind dynamic pressure increase causes a magnetic impulse on the ground with enhanced amplitude at the dayside geomagnetic equator [e.g., *Araki*, 1994]. Although the solar wind dynamic pressure shows quite a few irregular variations (Figure 7, top), three isolated impulsive changes (Figure 7, top, points 1–3) can be recognized clearly as a cause of magnetic impulses in the *DP* 2 fluctuations. The impulses in the two parameters coincide with each other within 1 min when shifted in time by 32 min. Under this condition, we also have excellent correspondence between the southward/northward IMF and the e-EJ/w-EJ in such a manner that the IMF/*DP* 2 crossed zero at 2213/2212, 2227/2228, 2242/2241, and 2304/2303 UT (Figure 7, middle, points a–d, respectively) in the plots of the IMF/*DP* 2. Note that the decrease in the *DP* 2 at 2320 UT must be caused by an electric field associated with a substorm, which is followed by the fluctuations during the storm main phase. Substorm-associated electric fields are an important issue to be studied in a separate paper. The excellent correspondence in both dynamic pressure and IMF variations with the *DP* 2 fluctuations validates the time shift of 32 min if we

Table 1. National Institute of Information and Communications Technology Space Weather Monitoring Magnetometer Stations

	Geographic Coordinates (°)		Geomagnetic Coordinates (°)		
Station	Latitude	Longitude	Latitude	Longitude	LT
Paratunka, Russia	52.94N	158.25E	45.58N	221.13E	UT + 10.6
Okinawa, Japan	26.75N	128.22E	16.87N	198.41E	UT + 8.4
Yap, Micronesia	9.49N	138.09E	0.38S	209.21E	UT + 9.2

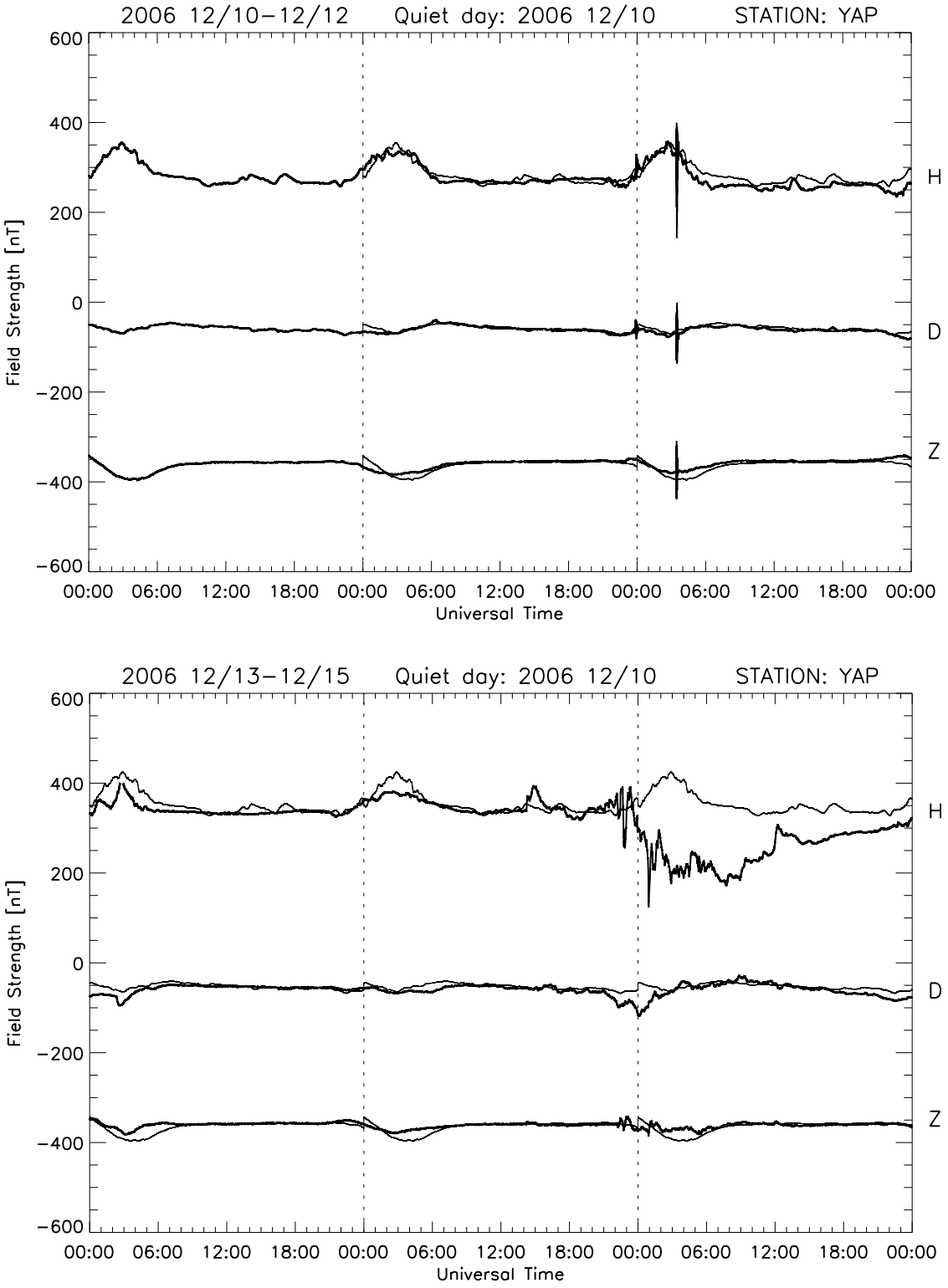

Figure 4. The *H*, *D*, and *Z* component magnetic fields recorded at YAP on 10–15 December 2006 (thick lines). The quiet-time diurnal curves on 10 December are plotted with thin lines.

allow 4.8 min for the interplanetary electric field (IEF) to propagate from the magnetopause to the equatorial ionosphere. Interestingly, *Manoj et al.* [2008] found that the time delay between the IEF and the equatorial electric field was less than 5 min on the basis of the statistical analysis of ionospheric drift measurements from the Jicamarca Unattended Long-term Investigations of the Ionosphere and Atmosphere radar. Consequently, the e-EJ was driven by the dawn-to-dusk convection electric field caused by the southward IMF, while the w-EJ must be caused by the over-

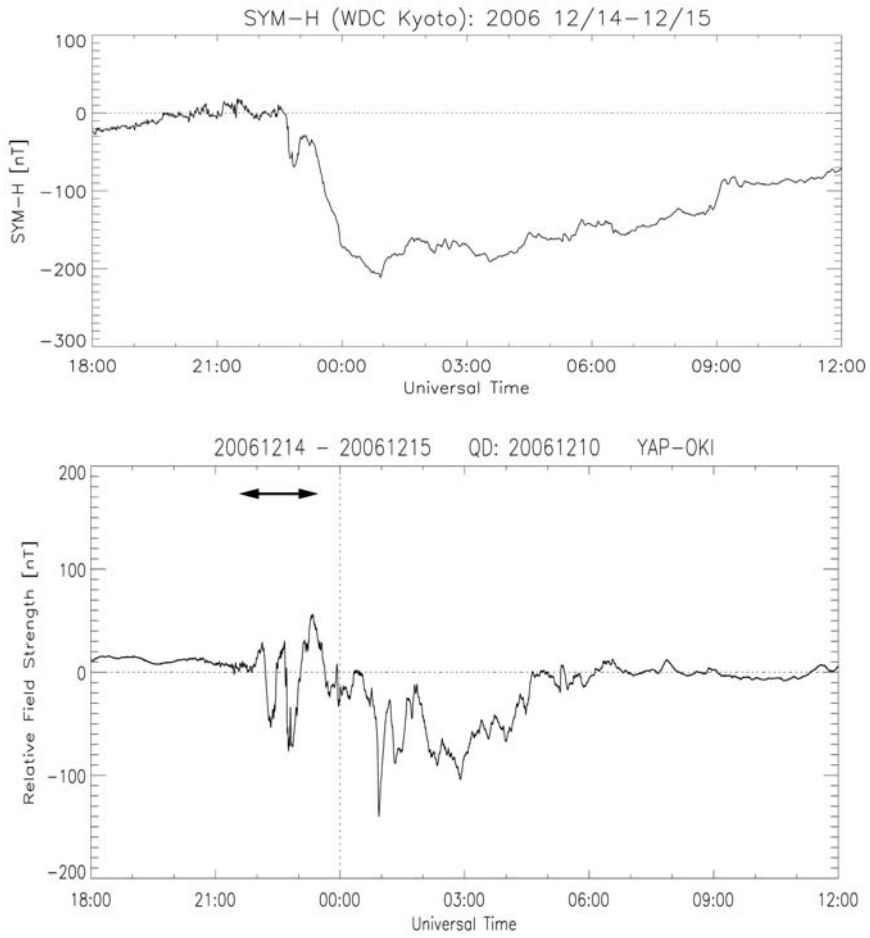

Figure 5. (bottom) *DP* 2 fluctuations derived from the *H* component magnetic fields at YAP and OKI along with (top) the SYM-H. The *DP* 2 fluctuations in the time interval of 2130–2330 UT, 14 December 2006 (double-headed arrow), are analyzed in section 2, and fluctuations in the time interval of 0000–0300 UT, 15 December, are discussed in section 3.

shielding electric field associated with the R2 FACs [*Nopper and Carovillano*, 1978; *Peymirat et al.*, 2000].

2.3. Super Dual Auroral Radar Network Convection Map

[13] To confirm that the w-EJ was caused by the overshielding electric field associated with the R2 FACs, we examined the ionospheric convection pattern derived from SuperDARN observations [*Ruohoniemi and Baker*, 1998]; SuperDARN is a global network of HF radars capable of measuring backscatter from drifting plasma in the ionospheric *F* region [*Greenwald et al.*, 1995]. Most of the SuperDARN radars have fields of view covering high-latitude regions. Therefore, the SuperDARN convection map reveals the large-scale convection pattern due to the R1 FACs. On the other hand, radars at King Salmon, Alaska (58.68°N, 156.65°W geographic; 57.43°N, 100.51°E Altitude Adjusted Corrected Geomagnetic Coordinates (AACGM)), and Hokkaido, Japan (43.53°N, 143.61°E geographic; 38.14°N, 145.67°W AACGM), cover a wide area of the subauroral region. These radars are suitable for acquiring convection patterns relevant to overshielding due to the R2 FACs.

[14] Figure 8 shows selected convection maps in the dayside polar ionosphere during the *DP* 2 fluctuation event; the inset indicates the IMF clock angle observed by ACE 32 min earlier. The direction of the convection flow is indicated by the arrows extending from the individual grid points. The flow speed is indicated by the color and length of the vector in accord with the given color code and 2 km s^{-1} bar. The flow vectors are aligned along the potential contours; positive potential is indicated with dashed contours and negative potential is indicated with solid contours. The radar coverage was limited to the dayside throughout the time interval of the *DP* 2 fluctuations, but the dayside part of the large-scale convection pattern is easily recognized in Figure 8. As shown, the convection forms a two-cell pattern under the condition of southward IMF, which is characterized by counterclockwise vortices in the morning sector (right-hand side of each panel in Figure 8) centered at about 75°N (Figures 8a, 8d, and 8f). These patterns are consistent with those derived from statistics of SuperDARN convection maps [*Ruohoniemi and Greenwald*, 1996]. The dawn-to-dusk electric field associated with the two-cell pattern penetrated to the equatorial ionosphere and caused the e-EJ shown in

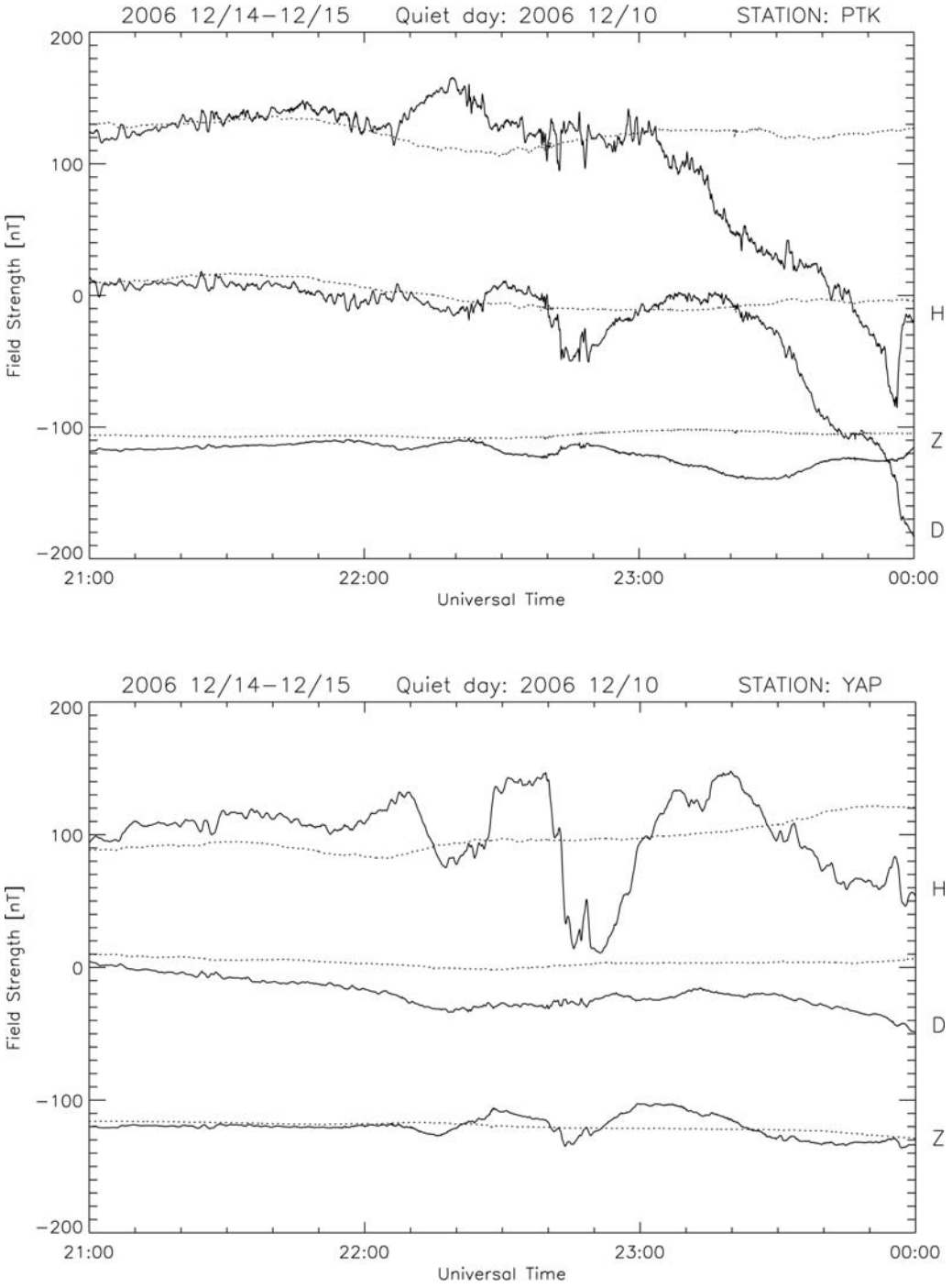

Figure 6. The *H*, *D*, and *Z* component magnetic fields recorded at PTK and YAP during the *DP* 2 fluctuation event on 14 December 2006. Quiet-time diurnal curves on 10 December 2006 are shown with dotted lines, as a reference for the *DP* 2 fluctuations.

Figure 7. On the other hand, the convection pattern became distorted considerably under the condition of northward IMF, which accompanied reverse flow vortices centered at about 67°N in the 0800 MLT meridian (Figures 8b, 8c, and 8e). The reverse vortices must be associated with the R2 FACs that developed equatorward of the R1 FACs. The dusk-to-dawn electric field associated with the R2 FACs penetrated to the equator and caused the w-EJ (Figure 7).

[15] Data for the reverse convection vortex in the morning sector was contributed mainly by the King Salmon radar. To evaluate this vortex, we analyzed data from the Hokkaido radar, which covered the field of view of the King Salmon radar during the *DP* 2 fluctuation event. Figure 9 shows line-of-sight (LOS) velocities measured by beam 9 of the Hokkaido radar. Positive LOS velocity during the periods 2210–2225 and 2240–2250 UT (green/blue) indicates short-

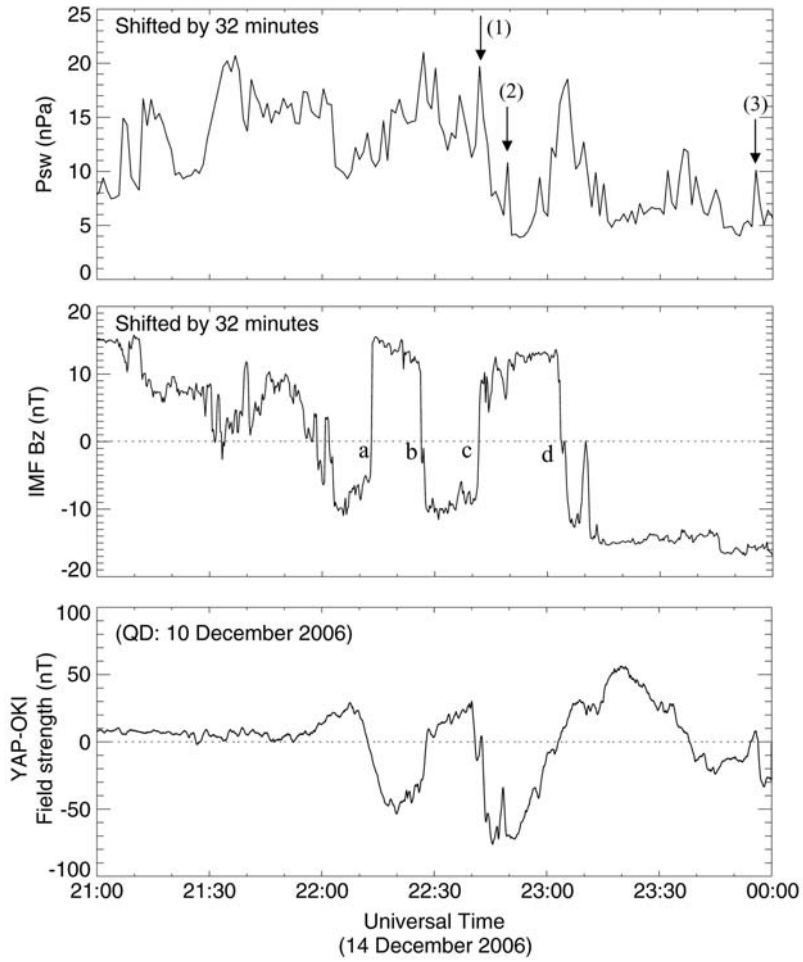

Figure 7. (top) Solar wind dynamic pressure, (middle) IMF B_z measured by ACE 32 min prior to the *DP* 2 fluctuation event, and (bottom) the *DP* 2 fluctuations derived from the *H* component magnetic fields at YAP and OKI. Solar wind dynamic pressure impulses numbered as 1–3 correspond to magnetic impulses in the *DP* 2 within 1 min. The IMF and *DP* 2 fluctuations crossed zero nearly at the same time within 1 min as indicated in Figure 7 (middle) by points a–d.

ening of the path length of HF radio propagation, which was primarily caused by a westward electric field through the E × B drift of ionospheric plasma. The westward electric field in the morning sector should be a part of the dusk-to-dawn electric field associated with the R2 FACs, which caused the w-EJ at the equator. The observed LOS velocity is very low compared with the auroral plasma flow [e.g., *Ruohoniemi and Baker*, 1998], probably because the radar signals were backscattered from the ground via the ionosphere. However, the Hokkaido radar can detect slow plasma flow associated with overshielding, as confirmed by *Ebihara et al.* [2008].

2.4. Comprehensive Ring Current Model Electric Potential

[16] We here calculate the electric potentials of the R1 and R2 FACs, using the CRCM [*Fok et al.*, 2001] to confirm the dominant contribution of the R2 FACs during the period of northward IMF. The simulation region is set from 11.8°N to 66.7°N magnetic latitude at the ionosphere altitude. The potential at the poleward boundary is imposed by using the empirical electric potential of *Weimer* [2001]. The electric potential model depends on the solar wind and IMF. Auroral conductance is provided by the *Hardy et al.* [1987] model depending on the *Kp* index, and background conductance is based on the Mass Spectrometer Incoherent Scatter (MSIS-E90) neutral atmosphere model [*Hedin*, 1991] and the international reference ionosphere (IRI-95) model [*Bilitza*, 1997]. The magnetic field is given by the 1996 model of Tsyganenko [*Tsyganenko*, 1995; *Tsyganenko and Stern*, 1996]. The distribution function of ions at the magnetosphere boundary is assumed to be isotropic Maxwellian with density of 0.75 cm^{-3} and temperature of 5 keV. All these parameter settings are the same as those of *Ebihara et al.* [2008], who simulated the same magnetic storm. We solve the advection of the energetic ions in the inner magnetosphere and the FACs flowing into/out from the ionosphere, which are referred to as the R2 FACs. The polarity of the electric potentials resulting from the R2 FACs is opposite to that of the polar cap potential (PCP).

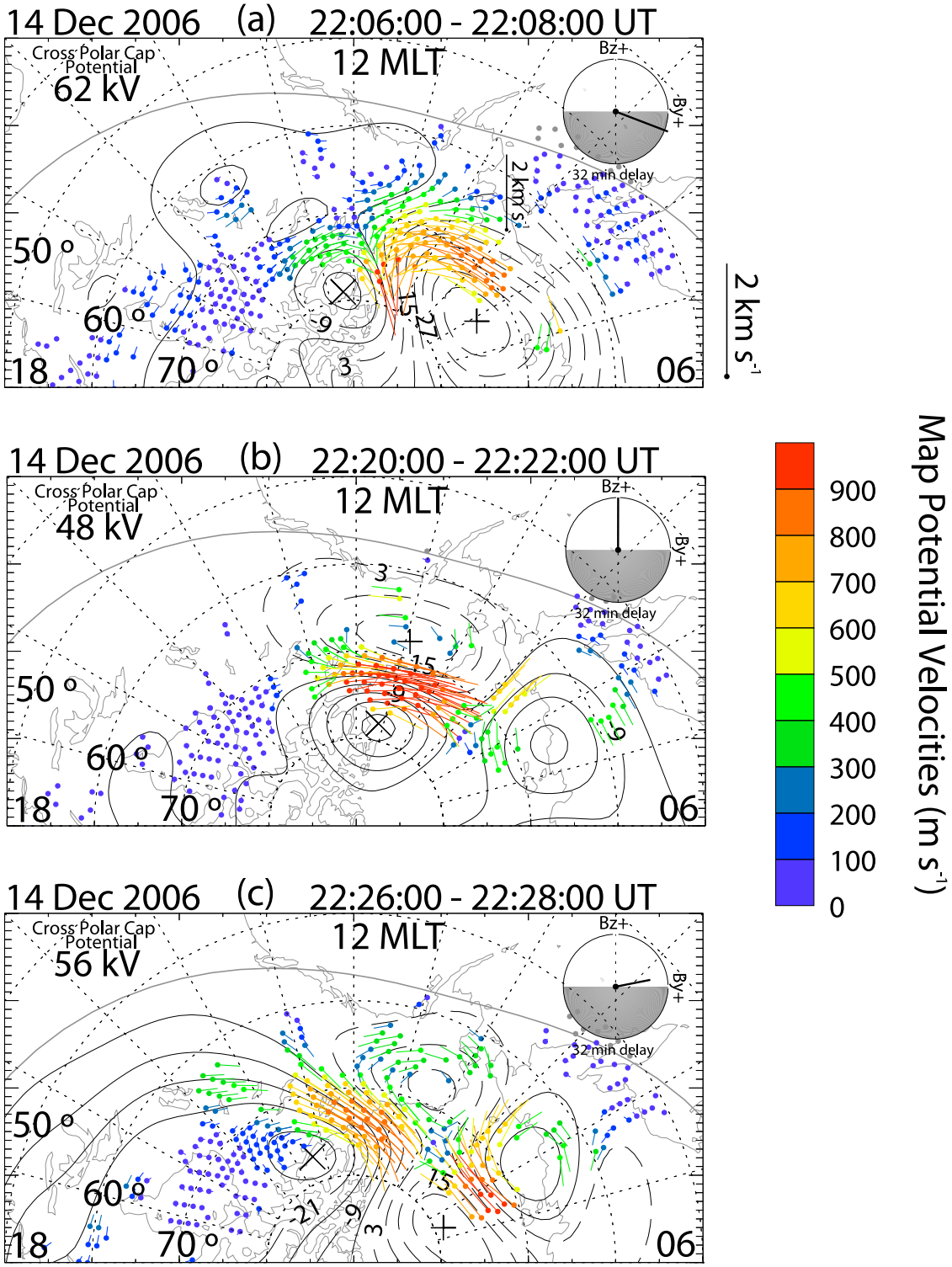

Figure 8. Super Dual Auroral Radar Network (SuperDARN) convection maps in the dayside polar ionosphere (>50°CGML), selected for (a, d, f) southward and (b, c, e) northward IMF conditions during the *DP* 2 fluctuation event. The colored arrows from the dots at individual grid points indicate vectors of ionospheric convection flow. The magnitude of the flow vector is indicated by the velocity bar and color code given. The positive (negative) electric potential is indicated by the dashed (solid) contours. (inset) IMF clock angle observed by ACE 32 min earlier.

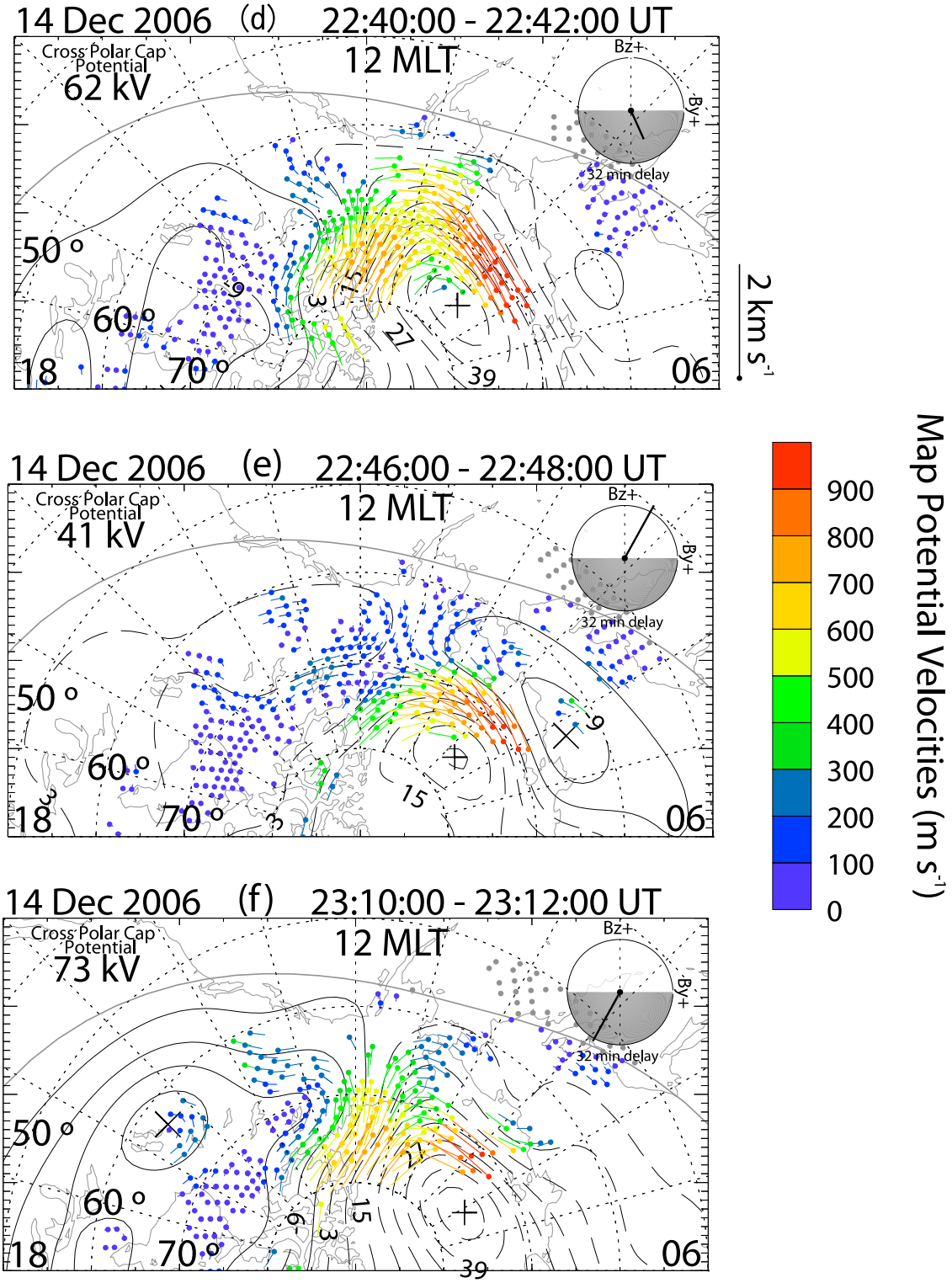

Figure 8. (continued)

[17] Figure 10 shows the density distribution of the R2 FACs, with warm (cool) colors for downward (upward) currents and contours of the sum of the PCP and the electric potential associated with the R2 FACs at the time indicated by the red line in the plots of the IMF B_z shifted in time by 32 min. The simulation results show that the electric potential contours are in a large-scale two-cell pattern associated with the R1 FACs under southward IMF (Figures 10a and

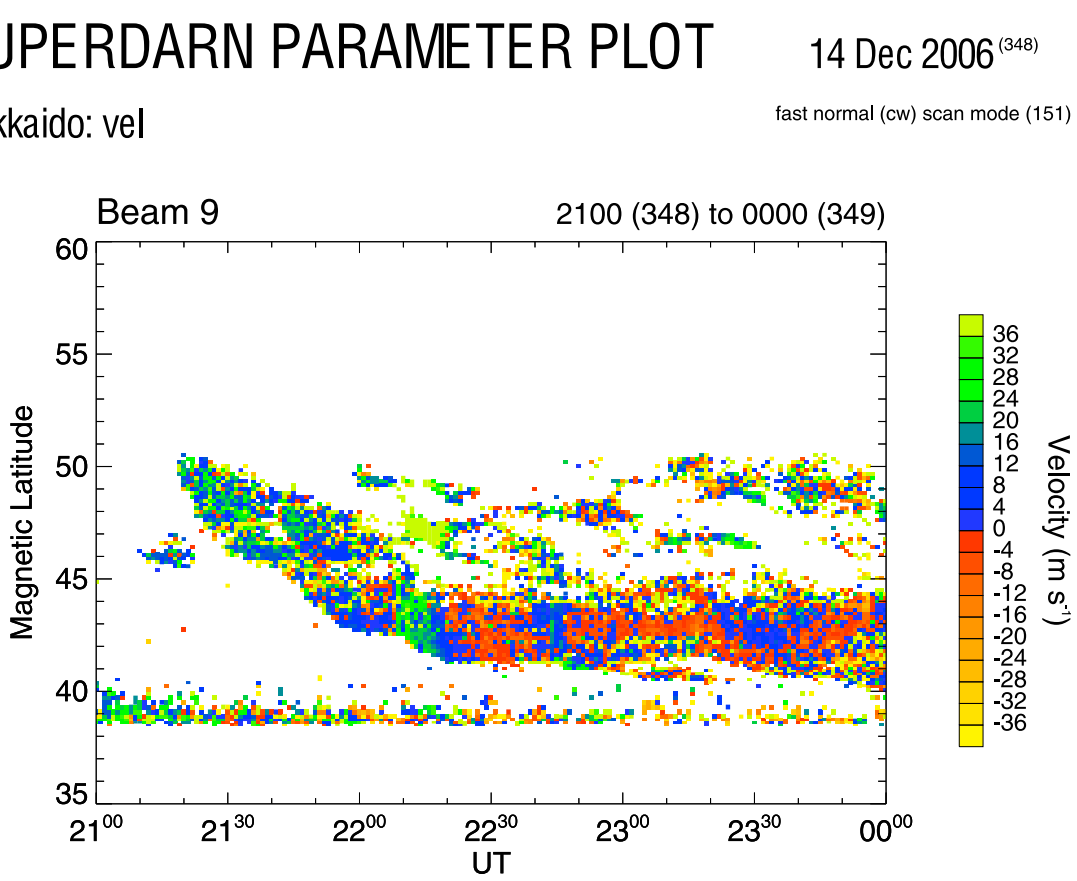

Figure 9. UT versus latitude plots of the line-of-sight velocity measured by beam 9 of the Hokkaido radar. Positive (green, blue) and negative (red, yellow) velocities indicate plasma motion toward and away from the radar caused by the westward and eastward electric fields, respectively.

10d). On the other hand, when the IMF turned northward, the electric potential was dominated by that of the R2 FACs (Figures 10b and 10e), which remained while the IMF B_z was positive (Figures 10c and 10f). As a result, electric potential contours surrounding the R2 FACs appear at around 0300 and 1500 MLT, which will cause the reversed convection vortices equatorward of the large-scale convection vortices as observed by SuperDARN (Figure 8) and the westward electric field at lower latitudes responsible for the w-EJ at the dayside equator. Note that the calculated R2 FAC-associated electric potential contours appear in the nightside morning sector (0300 MLT) but not on the dayside (0800 MLT), where the reverse convection vortex was observed by SuperDARN. The discrepancy between the observation and simulation raises an issue about the local time distribution of the asymmetric ring current and R2 FACs, which should be addressed in future works.

[18] To better understand the alternating appearance of the convection electric field (e-EJ) and overshielding electric field (w-EJ), we calculated the net R2 FAC and plotted it in Figure 11 (bottom, dotted lines) along with the PCP (solid lines). The IMF B_z is plotted in Figure 11 (top) with a time shift of 32 min. We find that the growth of the R2 FACs follows that of the PCP with some time lag, 6 min, as measured from the peak of the PCP to the peak of the net R2 FAC. The net R2 FAC decays more slowly than the PCP. As a result, the overshielding electric field due to the R2 FACs becomes dominant during the period of northward IMF.

3. Discussion and Conclusion

[19] The definition of *DP* 2 fluctuations has been controversial. *Matsushita and Balsley* [1972] pointed out that the *DP* 2 fluctuations should be measured as negative from the quiet-time diurnal curve with a time lag of several tens of minutes, since the daytime level of the diurnal curve on disturbed days has often been well below the quiet-time diurnal curve (see 13 and 14 December data in Figure 4). *Nishida* [1973], however, emphasized that there was no reason to believe that the convection electric field propagated to the equator so slowly as to be observed 20 min behind the high-latitude *DP* 2 fluctuations. In fact, the polar electric field propagates to the equator instantaneously with temporal resolution of 10 s during the preliminary impulse of geomagnetic sudden commencements [*Araki*, 1977; *Kikuchi*, 1986], which is caused by *DP* 2-type ionospheric currents. Furthermore, *Kikuchi et al.* [1996], using high-time-resolution magnetometer data, made a correlation analysis between high-latitude and equatorial *DP* 2 fluctuations (period = 40 min) and found that the equatorial *DP* 2 was positively correlated with that at high latitude (correlation coefficient, 0.9) and no time lag was greater than 25 s. In spite of the good correlation, however, we had no definitive idea about the true direction

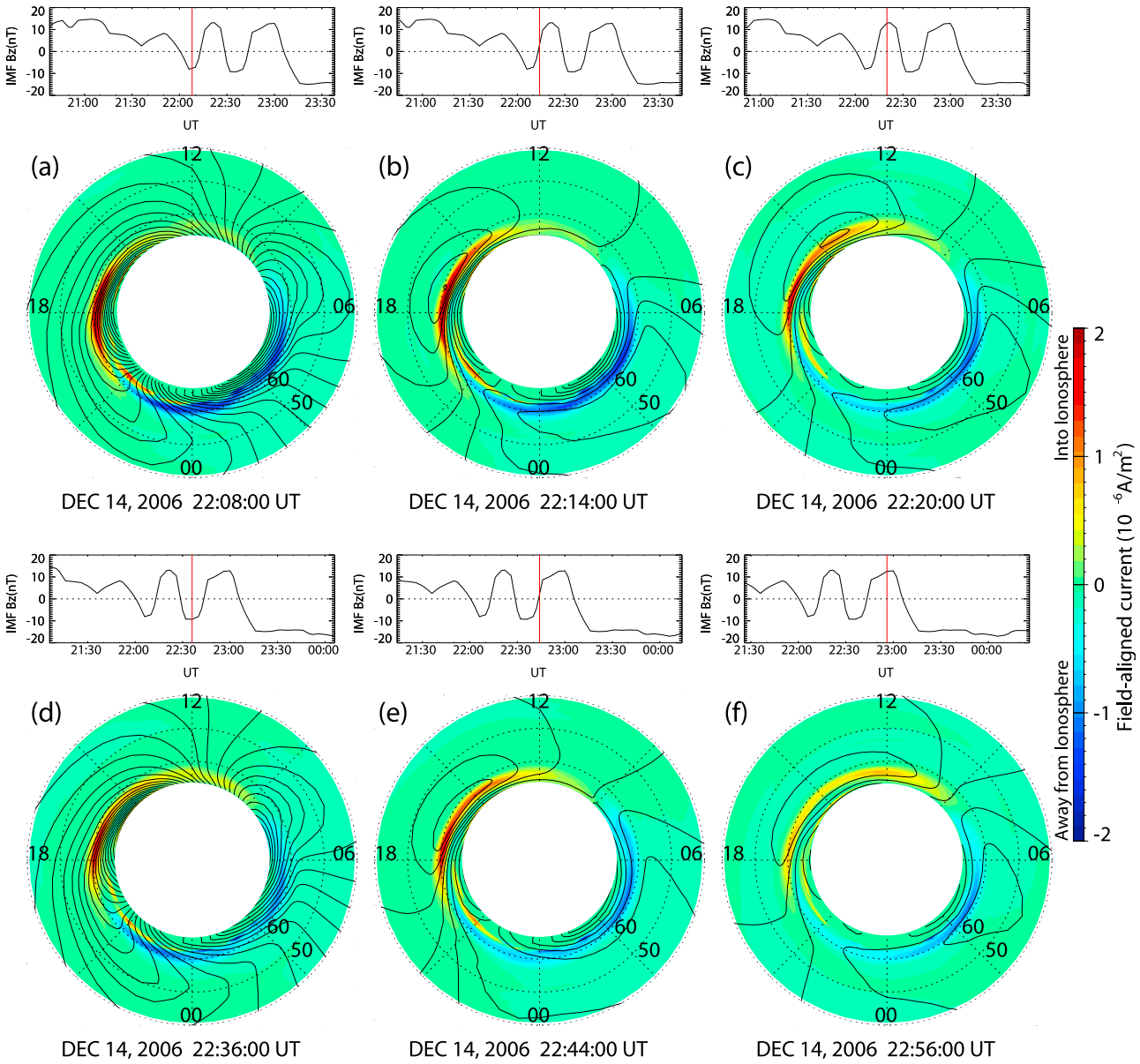

Figure 10. Current density of the region 2 field-aligned currents (R2 FACs) and contours of the electric potential calculated with the comprehensive ring current model (CRCM) at times indicated by red lines in the inset plots of the IMF B_z shifted in time by 32 min behind. Red (blue) indicates downward (upward) current density. The electric potential is calculated as a sum of the polar cap potential (PCP) and that of the R2 FACs.

of the ionospheric currents causing the *DP* 2 fluctuations. In the present study, we selected a *DP* 2 fluctuation event with a large amplitude (>100 nT from peak to peak) and no contamination of negative deflections attributable to the disturbance dynamo. The large amplitude of the *DP* 2 fluctuations enabled us to find the true direction of the equatorial electrojet: the *DP* 2 fluctuations were composed of alternating eastward and westward electrojets, which were caused by the southward and northward IMF, respectively.

[20] During geomagnetic storms, on the other hand, we often have difficulties in identifying the cause of *DP* 2 fluctuations. As shown in Figure 3, large-amplitude *DP* 2-like fluctuations occurred within the period 0000–0300 UT on 15 December 2006, during the storm main phase. Note that the IMF did not fluctuate but remained steadily southward (Figure 1); furthermore, the fluctuations were superposed by long-lasting negative deflections (Figure 5). These results imply that at least two different kinds of electric field contributed to the fluctuations during the main phase of a storm. One must be associated with a dynamo in the inner magnetosphere and the other linked with the disturbance dynamo in the thermosphere. *DP* 2-like fluctuations have often been observed during the main phase of a storm [*Fejer et al.*, 2007; *Veenadhari et al.*, 2010], when correlation with the IMF is

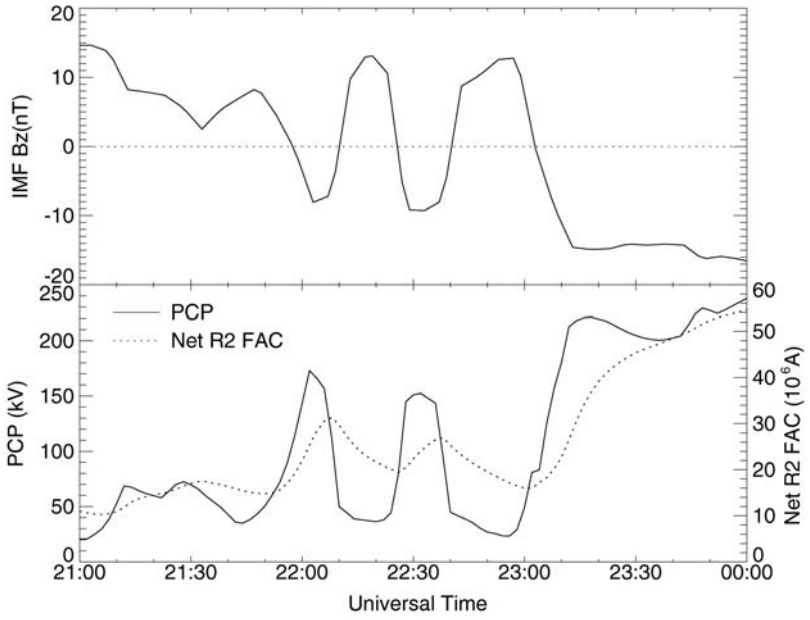

Figure 11. Plots of (top) the IMF B_z shifted in time by 32 min and (bottom) the PCP calculated with the empirical formula of *Weimer* [2001] (solid curve). The dotted curve in Figure 11 (bottom) indicates the net R2 FAC calculated using the CRCM with the PCP as an input.

not as good as that shown in this paper. Some other inner magnetosphere processes like substorms may play a role in the storm-time perturbations, an issue to be addressed in a separate paper.

[21] On the other hand, the disturbance dynamo electric field becomes dominant a few hours after the storm onset and remains for many hours, as deduced from the statistical studies of the equatorial electric field measured by the Jicamarca incoherent scatter radar [*Fejer and Scherliess*, 1997]. Simulation studies clarified the relative role of the prompt penetration and disturbance dynamo electric fields-*Maruyama et al.*, 2007]. Using the coupled thermosphere ionosphere plasmasphere electrodynamics (CTIPe) model, *Maruyama et al.* [2007] showed good agreement between model predictions and data, accounting for oscillations in the penetration electric field at the beginning of the storm on 31 March 2001 and the disturbance dynamo electric field during the storm main phase. We stress that the *DP* 2 fluctuations studied in section 2 occurred just before the storm-associated dynamos started to work. Application of the CTIPe model would be useful to evaluate our scenario, and should be a next step in studying the penetration electric field.

[22] We further attempted to find similar *DP* 2 fluctuation events to confirm the close relationship between the *DP* 2 and IMF fluctuations. Figures 12 and 13 show *DP* 2 fluctuations observed during geomagnetic storms on 6–7 June 2006 and 7–8 May 2005. Solar wind parameters are plotted in Figures 12 (top) and 13 (top) and the *DP* 2 fluctuations in Figures 12 (bottom) and 13 (bottom), which are in the same format as in Figures 1 and 5, respectively. The *DP* 2 fluctuations in the first event have rather good correlations with fluctuations in southward IMF (Figure 12). However, we could not use this event to confirm whether the *DP* 2 fluctuations were composed of alternating e-EJ and w-EJ because the small amplitude (<70 nT, peak to peak) of the *DP* 2 fluctuations were overwhelmed by the large negative depression of the daytime level (>−100 nT).

[23] In the second event (Figure 13), on the other hand, the *DP* 2 fluctuations have a large amplitude (<130 nT, peak to peak) superposed by a small negative depression (>−30 nT). Therefore, we can confirm that the *DP* 2 fluctuations are composed of alternating e-EJ and w-EJ in the same manner as in section 2. However, the correlation of the *DP* 2 fluctuations with the IMF is not so clear as in the event analyzed in section 2. Several impulsive northward turnings between 2030 UT on 7 May and 0030 UT on 8 May could have contributed to the w-EJ between 2130 and 0130 UT. We stress again that the *DP* 2 fluctuations studied in section 2 are remarkably well correlated with the IMF fluctuations (Figure 7).

[24] It seems commonly accepted that the dawn-to-dusk ionospheric electric field is attributed to the solar wind electric field. If this is always true, the westward electric field in the equatorial ionosphere responsible for the w-EJ must be caused by the solar wind electric field associated with the northward IMF. The SuperDARN convection map, however, indicated that the convection pattern was not a two-cell pattern with reversed polarity but instead was composed of distorted double cells or multiple cells in agreement with the statistically obtained convection patterns [*Heppner and Maynard*, 1987; *Weimer*, 2001; *Ruohoniemi and Greenwald*, 1996]. Moreover, we revealed that reverse flow vortices appearing at lower latitudes will produce a reverse electric field, i.e., an overshielding electric field, at middle and low latitudes. CRCM calculations show that the

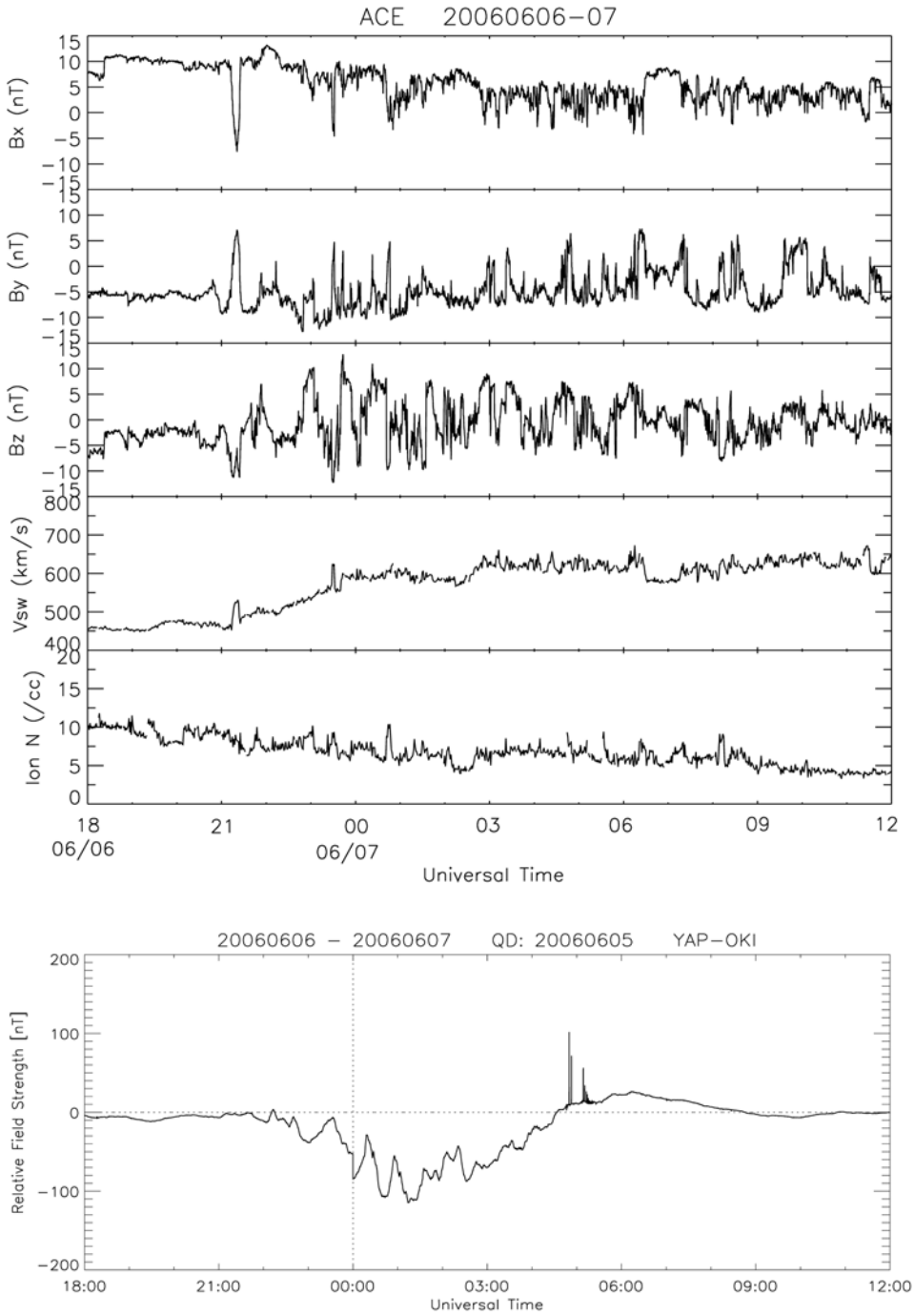

Figure 12. Solar wind parameters measured by ACE and the equatorial *DP* 2 fluctuations during the geomagnetic storm on 6–7 June 2006, shown in the same formats as in Figures 1 and 5, respectively.

electric potential associated with the R2 FACs overcomes that associated with the R1 FACs when the IMF turns northward, which results in reverse convection vortices equatorward of the large-scale two-cell convection vortices. The calculated reverse convection vortices are consistent with the flow observed at subauroral and midlatitudes by the King Salmon and Hokkaido radars (Figures 8 and 9), except for the local time. Finally, the overshielding electric field caused the w-EJ of the *DP* 2 fluctuations at the equator. From an electric current point of view, the R1 and R2 FACs flowed into the equatorial ionosphere alternately and caused the e-EJ and w-EJ, respectively.

[25] CRCM calculations indicated that the shielding electric field started to develop immediately after the growth of the PCP but with a time lag of 6 min in peak intensity. The R2 FACs decayed more gradually than the PCP (Figure 11). As a result, the shielding electric field overwhelmed the convection electric field; overshielding occurred as the con-

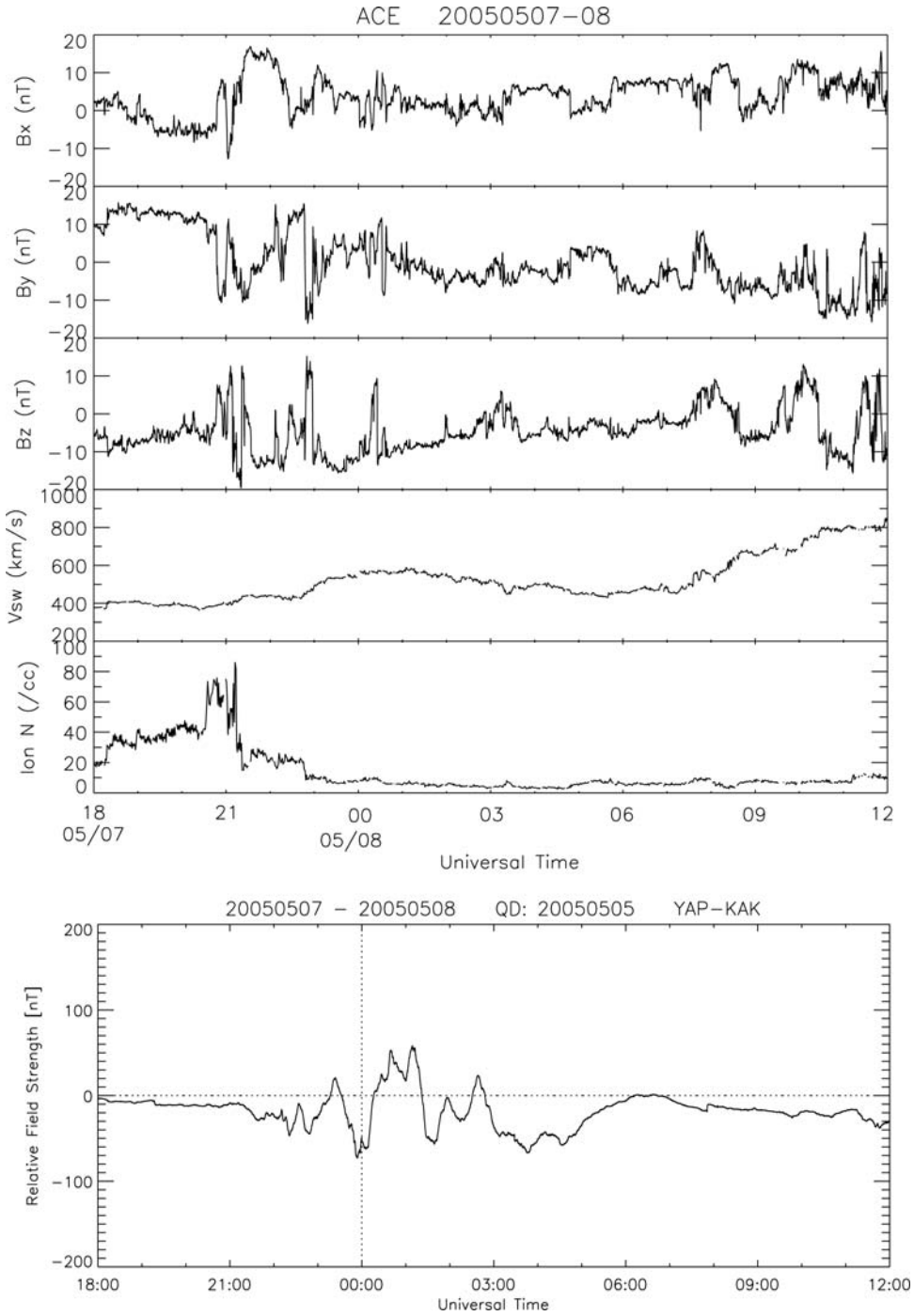

Figure 13. Solar wind parameters measured by ACE and the equatorial *DP* 2 fluctuations during the geomagnetic storm on 7–8 May 2005, shown in the same formats as in Figure 12.

vection electric field decreased. We stress that shielding/overshielding occurs for both short- and long-period fluctuations, i.e., *DP* 2 fluctuations of 30 min period (this study), substorm growth phase [*Somayajulu et al.*, 1987], substorm recovery phase [*Kelley et al.*, 1979; *Kobea et al.*, 2000; *Kikuchi et al.*, 2000, 2003], and storm recovery phase [*Kikuchi et al.*, 2008a,b]. On the other hand, shielding is not effective during the period of growing R1 FACs. Thus, the convection electric field can be dominant for several hours during storm main phase, as demonstrated by *Huang et al.* [2005, 2007].

[26] In conclusion, the equatorial *DP* 2 fluctuations are caused by alternating e-EJ and w-EJ connecting with the R1 and R2 FACs, being driven by the southward and northward IMF, respectively. The R2 FACs develop immediately after the growth of the R1 FACs but decay more gradually with some time lag (6 min), according to the CRCM calculation. Thus, overshielding due to the dominant R2 FACs occurs

whenever the R1 FACs decrease rapidly. The period of alternate development of the two FAC systems is 30–60 min for *DP* 2 fluctuation events and much longer for geomagnetic storms.

[27] **Acknowledgments.** We would like to thank the Institute of Cosmophysical Research and Radio Wave Propagation (IKIR), the U.S. NOAA/Weather Service Office at Yap, and Ryukyu University for their help in operating the NICT space weather monitoring magnetometers at Paratunka, Yap, and Okinawa, respectively. The SYM-H was provided by the World Data Center for Geomagnetism, Kyoto. The ACE solar wind data were obtained through the Coordinated Data Analysis Web (CDAWeb). The CRCM simulation code was kindly provided by Mei-Ching Fok at NASA/GSFC. The work of YE is supported by the Program for Improvement of Research Environment for Young Researchers from the Special Coordination Funds for Promoting Science and Technology (SCF) commissioned by the Ministry of Education, Culture, Sports, Science and Technology (MEXT) of Japan.

[28] Wolfgang Baumjohann thanks Atsuhiro Nishida and two other reviewers for their assistance in evaluating this manuscript.

References

Araki, T. (1977), Global structure of geomagnetic sudden commencements, *Planet. Space Sci.*, *25*, 373–384, doi:10.1016/0032-0633(77)90053-8.

Araki, T. (1994), A physical model of geomagnetic sudden commencement, in *Solar Wind Sources of Magnetospheric Ultra-Low-Frequency Waves*, *Geophys. Monogr. Ser.*, vol. 81, edited by M. J. Engebretson, K. Takahashi, and M. Scholer, pp. 183–200, AGU, Washington, D. C.

Bilitza, D. (1997), International reference ionosphere: Status, 1995/96, *Adv. Space Res.*, *20*, 1751, doi:10.1016/S0273-1177(97)00584-X.

Blanc, M., and A. D. Richmond (1980), The ionospheric disturbance dynamo, *J. Geophys. Res.*, *85*, 1669–1686, doi:10.1029/JA085iA04p01669.

Ebihara, Y., N. Nishitani, T. Kikuchi, T. Ogawa, K. Hosokawa, and M.-C. Fok (2008), Two-dimensional observations of overshielding during a magnetic storm by the Super Dual Auroral Radar Network (SuperDARN) Hokkaido radar, *J. Geophys. Res.*, *113*, A01213, doi:10.1029/2007JA012641.

Fejer, B. G., and L. Scherliess (1997), Empirical models of storm time equatorial zonal electric fields, *J. Geophys. Res.*, *102*, 24,047–24,056, doi:10.1029/97JA02164.

Fejer, B. G., C. A. Gonzales, D. T. Farley, and M. C. Kelley (1979), Equatorial electric fields during magnetically disturbed conditions: 1. The effect of the interplanetary magnetic field, *J. Geophys. Res.*, *84*, 5797–5802, doi:10.1029/JA084iA10p05797.

Fejer, B. G., J. W. Jensen, T. Kikuchi, M. A. Abdu, and J. L. Chau (2007), Equatorial ionospheric electric fields during the November 2004 magnetic storm, *J. Geophys. Res.*, *112*, A10304, doi:10.1029/2007JA012376.

Fok, M.-C., R. A. Wolf, R. W. Spiro, and T. E. Moore (2001), Comprehensive computational model of Earth's ring current, *J. Geophys. Res.*, *106*, 8417–8424, doi:10.1029/2000JA000235.

Gonzales, C. A., M. C. Kelley, B. G. Fejer, J. F. Vickrey, and R. F. Woodman (1979), Equatorial electric fields during magnetically disturbed conditions: 2. Implications of simultaneous auroral and equatorial measurements, *J. Geophys. Res.*, *84*, 5803–5812, doi:10.1029/JA084iA10p05803.

Greenwald, R. A., et al. (1995), DARN/SuperDARN: A global view of high-latitude convection, *Space Sci. Rev.*, *71*, 761–796, doi:10.1007/BF00751350.

Hardy, D. A., M. S. Gussenhoven, R. Raistrick, and W. J. McNeil (1987), Statistical and functional representations of the pattern of auroral energy flux, number flux, and conductivity, *J. Geophys. Res.*, *92*, 12,275–12,294, doi:10.1029/JA092iA11p12275.

Hedin, A. E. (1991), Extension of the MSIS thermospheric model into the middle and lower atmosphere, *J. Geophys. Res.*, *96*, 1159, doi:10.1029/90JA02125.

Heppner, J., and N. Maynard (1987), Empirical high-latitude electric field models, *J. Geophys. Res.*, *92*, 4467–4489, doi:10.1029/JA092iA05p04467.

Huang, C.-S., J. C. Foster, and M. C. Kelley (2005), Long-duration penetration of the interplanetary electric field to the low-latitude ionosphere during the main phase of magnetic storms, *J. Geophys. Res.*, *110*, A11309, doi:10.1029/2005JA011202.

Huang, C.-S., S. Sazykin, J. L. Chau, N. Maruyama, and M. C. Kelley (2007), Penetration electric fields: Efficiency and characteristic time scale, *J. Atmos. Sol. Terr. Phys.*, *69*, 1135–1146, doi:10.1016/j.jastp.2006.08.016.

Jaggi, R., and R. Wolf (1973), Self-consistent calculation of the motion of a sheet of ions in the magnetosphere, *J. Geophys. Res.*, *78*(16), 2852–2866, doi:10.1029/JA078i016p02852.

Kelley, M. C., B. G. Fejer, and C. A. Gonzales (1979), An explanation for anomalous equatorial ionospheric electric fields associated with a northward turning of the interplanetary magnetic field, *Geophys. Res. Lett.*, *6*, 301–304, doi:10.1029/GL006i004p00301.

Kikuchi, T. (1986), Evidence of transmission of polar electric fields to the low latitude at times of geomagnetic sudden commencements, *J. Geophys. Res.*, *91*, 3101–3105, doi:10.1029/JA091iA03p03101.

Kikuchi, T., H. Luehr, T. Kitamura, O. Saka, and K. Schlegel (1996), Direct penetration of the polar electric field to the equator during a *DP* 2 event as detected by the auroral and equatorial magnetometer chains and the EISCAT radar, *J. Geophys. Res.*, *101*, 17,161–17,173, doi:10.1029/96JA01299.

Kikuchi, T., H. Luehr, K. Schlegel, H. Tachihara, M. Shinohara, and T.-I. Kitamura (2000), Penetration of auroral electric fields to the equator during a substorm, *J. Geophys. Res.*, *105*, 23,251–23,261, doi:10.1029/2000JA900016.

Kikuchi, T., K. K. Hashimoto, T.-I. Kitamura, H. Tachihara, and B. Fejer (2003), Equatorial counterelectrojets during substorms, *J. Geophys. Res.*, *108*(A11), 1406, doi:10.1029/2003JA009915.

Kikuchi, T., K. K. Hashimoto, and K. Nozaki (2008a), Penetration of magnetospheric electric fields to the equator during a geomagnetic storm, *J. Geophys. Res.*, *113*, A06214, doi:10.1029/2007JA012628.

Kikuchi, T., K. K. Hashimoto, and K. Nozaki (2008b), Storm phase dependence of penetration of magnetospheric electric fields to mid and low latitudes, in *Midlatitude Ionospheric Dynamics and Disturbances, AGU Geophys. Monogr. Ser.*, vol. 181, edited by P. M. Kintner Jr., A. J. Coster, T. Fuller-Rowell, A. J. Mannucci, M. Mendillo, and R. Heelis, pp. 145–155, AGU, Washington, D. C.

Kobea, A. T., C. Amory-Mazaudier, J. M. Do, H. Luehr, E. Hougninou, J. Vassal, E. Blanc, and J. J. Curto (1998), Equatorial electrojet as part of the global circuit: A case-study from the IEEY, *Ann. Geophys.*, *16*, 698–710, doi:10.1007/s00585-998-0698-1.

Kobea, A. T., A. D. Richmond, B. A. Emery, C. Peymirat, H. Luehr, T. Moretto, M. Hairston, and C. Amory-Mazaudier (2000), Electrodynamic coupling of high and low latitudes: Observations on May 27, 1993, *J. Geophys. Res.*, *105*, 22,979–22,989, doi:10.1029/2000JA000058.

Manoj, C., S. Maus, H. Luehr, and P. Alken (2008), Penetration characteristics of the interplanetary electric field to the daytime equatorial ionosphere, *J. Geophys. Res.*, *113*, A12310, doi:10.1029/2008JA013381.

Maruyama, N., S. Sazykin, R. W. Spiro, D. Anderson, A. Anghel, R. A. Wolf, and F. R. Toffoletto (2007), Modeling storm-time electrodynamics of the low-latitude ionosphere-thermosphere system: Can long lasting disturbance electric fields be accounted for? *J. Atmos. Sol. Terr. Phys.*, *69*, 1182–1199.

Matsushita, S., and B. B. Balsley (1972), A question of *DP* 2 magnetic fluctuations, *Planet. Space Sci.*, *20*, 1259–1267, doi:10.1016/0032-0633(72)90013-X.

Nishida, A. (1968), Coherence of geomagnetic *DP* 2 magnetic fluctuations with interplanetary magnetic variations, *J. Geophys. Res.*, *73*, 5549–5559, doi:10.1029/JA073i017p05549.

Nishida, A. (1973), Reply to "A question of *DP* 2 magnetic fluctuations" by S. Matsushita and B. B. Balsley, *Planet. Space Sci.*, *21*, 1255–1259, doi:10.1016/0032-0633(73)90210-9.

Nishida, A., N. Iwasaki, and T. Nagata (1966), The origin of fluctuations in the equatorial electrojet; A new type of geomagnetic variation, *Ann. Geophys.*, *22*, 478–484.

Nopper, R., and R. Carovillano (1978), Polar-equatorial coupling during magnetically active periods, *Geophys. Res. Lett.*, *5*, 699–702, doi:10.1029/GL005i008p00699.

Onwumechilli, A., K. Kawasaki, and S.-I. Akasofu (1973), Relationships between the equatorial electrojet and polar magnetic variations, *Planet. Space Sci.*, *21*, 1–16, doi:10.1016/0032-0633(73)90015-9.

Peymirat, C., A. D. Richmond, and A. T. Kobea (2000), Electrodynamic coupling of high and low latitudes: Simulations of shielding/overshielding effects, *J. Geophys. Res.*, *105*, 22,991–23,003, doi:10.1029/2000JA000057.

Ruohoniemi, J., and K. Baker (1998), Large-scale imaging of high-latitude convection with Super Dual Auroral Radar Network HF radar observations, *J. Geophys. Res.*, *103*, 20,797–20,811, doi:10.1029/98JA01288.

Ruohoniemi, J., and R. Greenwald (1996), Statistical patterns of high-latitude convection obtained from Goose Bay HF radar observations, *J. Geophys. Res.*, *101*, 21,743–21,763, doi:10.1029/96JA01584.

Senior, C., and M. Blanc (1984), On the control of magnetospheric convection by the spatial distribution of ionospheric conductivities, *J. Geophys. Res.*, *89*, 261–284, doi:10.1029/JA089iA01p00261.

Somayajulu, V. V., C. A. Reddy, and K. S. Viswanathan (1987), Penetration of magnetospheric convective electric field to the equatorial iono-

sphere during the substorm of March 22, 1979, *Geophys. Res. Lett.*, *14*, 876–879, doi:10.1029/GL014i008p00876.

Southwood, D. (1977), The role of hot plasma in magnetospheric convection, *J. Geophys. Res.*, *82*, 5512–5520, doi:10.1029/JA082i035p05512.

Tsyganenko, N. A. (1995), Modeling the Earth's magnetospheric magnetic field confined within a realistic magnetopause, *J. Geophys. Res.*, *100*, 5599–5612.

Tsyganenko, N. A., and D. P. Stern (1996), A new-generation global magnetosphere field model, based on spacecraft magnetometer data, *ISTP Newsl.*, *6*(1), 21.

Vasyliunas, V. M. (1972), The interrelationship of magnetospheric processes, in *Earth's Magnetospheric Processes*, edited by B. M. McCormac, pp. 29–38, Reidel, Dordrecht, The Netherlands.

Veenadhari, B., S. Alex, T. Kikuchi, A. Shinbori, R. Singh, and E. Chandrasekhar (2010), Penetration of magnetospheric electric fields to the equator and their effects on low latitude ionosphere during intense geomagnetic storms, *J. Geophys. Res.*, *115*, A03305, doi:10.1029/2009JA014562.

Weimer, D. R. (2001), An improved model of ionospheric electric potentials including substorm perturbations and application to the Geospace Environment Modeling November 24, 1996, event, *J. Geophys. Res.*, *106*, 407–416, doi:10.1029/2000JA000604.

Y. Ebihara, Advanced Research Institute, Nagoya University, Furo-cho, Chikusa-ku, Nagoya, Aichi 464-8601, Japan.

K. K. Hashimoto, Kyushu University of Health and Welfare, Nobeoka, Miyazaki 882-8508, Japan.

T. Hori, T. Kikuchi, and N. Nishitani, Solar-Terrestrial Environment Laboratory, Nagoya University, Furo-cho, Chikusa-ku, Nagoya, Aichi 464-8601, Japan. (kikuchi@stelab.nagoya-u.ac.jp)

R. Kataoka, Computational Astrophysics Laboratory, Institute of Physics and Chemical Research (RIKEN), Wako, Saitama 351-0198, Japan.

S. Watari, National Institute of Information and Communications Technology, Koganei, Tokyo 184-8795, Japan.